LETTER

nature cell biology

Directing human embryonic stem cell differentiation towards a renal lineage generates a self-organizing kidney

M. Takasato[1], P. X. Er[1], M. Becroft[1], J. M. Vanslambrouck[1], E. G. Stanley[2,3], A. G. Elefanty[2,3] and M. H. Little[1,4]

With the prevalence of end-stage renal disease rising 8% per annum globally[1], there is an urgent need for renal regenerative strategies. The kidney is a mesodermal organ that differentiates from the intermediate mesoderm (IM) through the formation of a ureteric bud (UB) and the interaction between this bud and the adjacent IM-derived metanephric mesenchyme[2] (MM). The nephrons arise from a nephron progenitor population derived from the MM (ref. 3). The IM itself is derived from the posterior primitive streak[4]. Although the developmental origin of the kidney is well understood[2], nephron formation in the human kidney is completed before birth[5]. Hence, there is no postnatal stem cell able to replace lost nephrons. In this study, we have successfully directed the differentiation of human embryonic stem cells (hESCs) through posterior primitive streak and IM under fully chemically defined monolayer culture conditions using growth factors used during normal embryogenesis. This differentiation protocol results in the synchronous induction of UB and MM that forms a self-organizing structure, including nephron formation, *in vitro*. Such hESC-derived components show broad renal potential *ex vivo*, illustrating the potential for pluripotent-stem-cell-based renal regeneration.

On the basis of described embryology, we have defined a three-stage framework for the differentiation of hESCs to the key cellular compartments of the developing kidney, including genes that mark or exclude a specific end result[6] (Fig. 1a). The primitive streak, the progenitor population for both mesoderm and endoderm, can be induced from mouse ESCs (mESCs) using activin A (ref. 7) with opposing gradients of BMP4 and activin A specifying anterior (endoderm) versus posterior (mesoderm) primitive streak in mice[8,9]. Canonical Wnt signalling has also been reported as an inducer for primitive streak in mESCs and hESCs (refs 7,10). As the IM initially arises from the posterior primitive streak, we first examined whether hESCs responded to these morphogens in a similar way to mice. We have previously shown that 20:100 (ng ml^{-1}) of BMP4/activin A induced GFP$^+$ primitive streak from the reporter hESC line *MIXL1*$^{GFP/wt}$, in which GFP is knocked into the *MIXL1* gene locus, a robust marker of primitive streak[11]. Using this reporter line in monolayer culture, we tested several combinations of BMP4 and activin A (5:200, 20:100, 30:10, 30:0 and 0 : 0 ng ml^{-1}) or varying concentrations of a canonical Wnt signalling agonist, CHIR99021 (5, 7, 9 μM) for optimal differentiation. All *in vitro* experiments were performed under chemically defined serum-free culture conditions[12]. Comparative expression of *MIXL1*, *T* (posterior primitive streak) and *SOX17* (anterior primitive streak) suggested that high BMP4/low activin A (30:10) or high CHIR99021 (>7 μM) was optimal for posterior primitive streak (Fig. 1c,d and Supplementary Fig. 1a–c). Under both conditions, approximately 90% of cells became GFP$^+$ (Fig. 1b).

The second stage of differentiation was to induce IM from primitive streak. After gastrulation, the definitive mesoderm can give rise to IM, paraxial (PM) and lateral plate mesoderm (LPM). Previous studies investigating renal differentiation of pluripotent cells have relied on *OSR1* as a definitive marker of IM and even MM formation[13]. However, *OSR1* expression is seen in trunk mesoderm and extends into LPM (ref. 14). Spontaneous differentiation after initial induction of primitive streak (BMP4/activin A (30:10), 3 days) showed *OSR1* expression (Supplementary Fig. 1d) but no evidence of more definitive IM markers, *PAX2* and *LHX1* (refs 14–16), by either PCR with reverse transcription (RT–PCR) or immunofluorescence. This indicated a need for further growth factors to appropriately direct the next stage. FGF signalling was one possible requirement. FGF8 is expressed from primitive streak through to posterior trunk mesoderm and FGF9 is expressed in IM and PM (refs 17,18). MM survival *in vitro* is supported by

[1]Institute for Molecular Bioscience, The University of Queensland, St Lucia 4072, Queensland, Australia. [2]Murdoch Childrens Research Institute, The Royal Children's Hospital, Flemington Road, Parkville 3052, Victoria, Australia. [3]Department of Anatomy and Developmental Biology, Monash University, Wellington Road, Clayton 3800, Victoria, Australia.
[4]Correspondence should be addressed to M.H.L. (e-mail: M.Little@imb.uq.edu.au)

Received 23 January 2013; accepted 18 November 2013; published online 15 December 2013; DOI: 10.1038/ncb2894

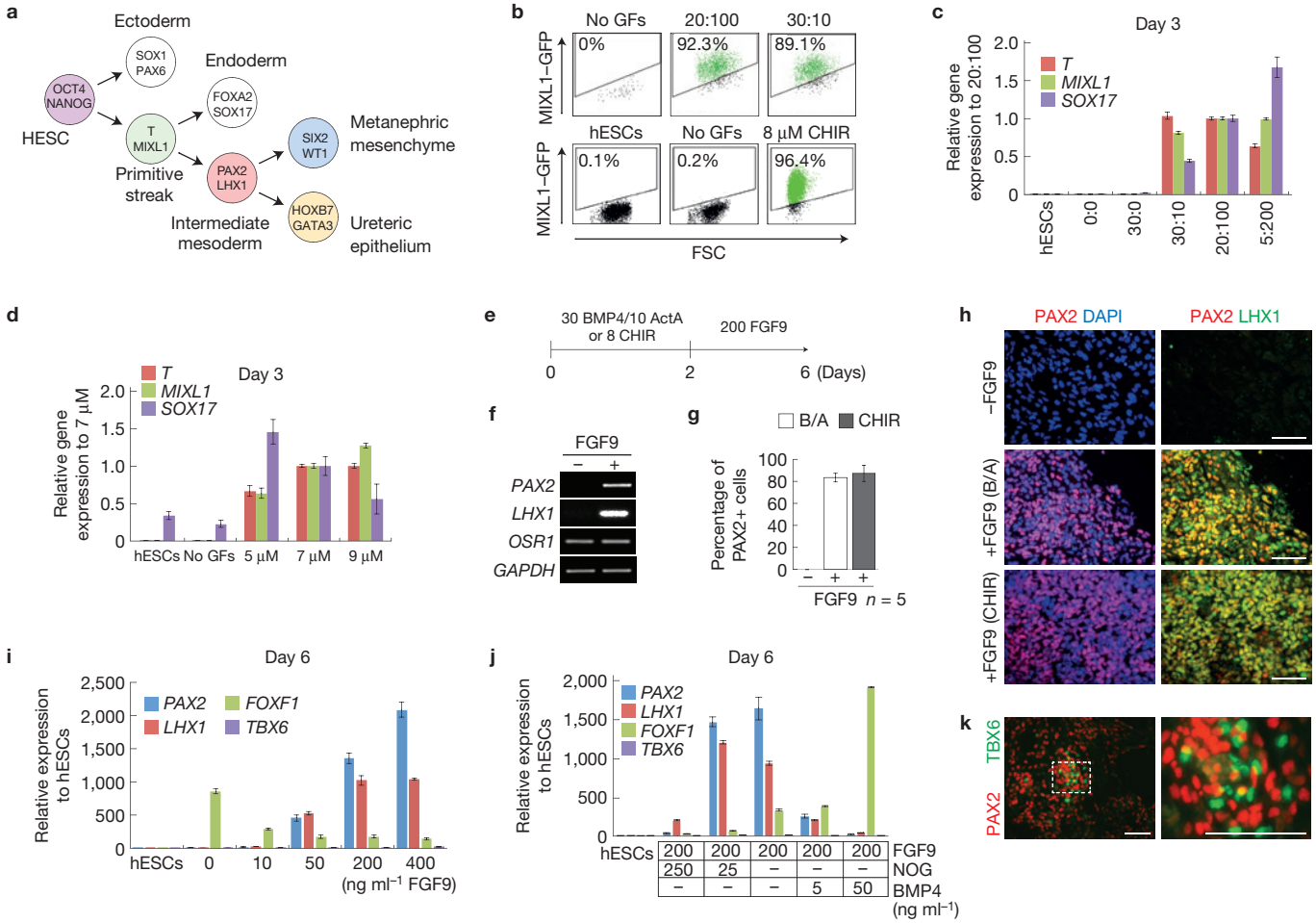

Figure 1 Sequential differentiation of primitive streak and intermediate mesoderm from human ESCs. (**a**) Schematic of developmental stages from inner cell mass to renal lineages. Genes shown in each stage represent specific markers of that stage. (**b**) FACS analysis (GFP and forward scatter (FSC)) showing the percentage of MIXL1–GFP-positive primitive streak cells induced with different ratios of BMP4/activin A (ng ml^{-1}) or 8 μM of CHIR99021 after 3 days of culture. hESC, starting cells; No GFs (growth factors), 3 days culture with basal media. (**c**) Relative expression levels of *SOX17*, brachyury (*T*) and *MIXL1* at day 3 for each ratio of BMP4 and activin A (ng ml^{-1}) assessed by qRT–PCR analysis). (**d**) The same qRT–PCR analysis for different concentrations of CHIR99021. Error bars are s.d. ($n = 3$ experiments). (**e**) Schematic representation of the differentiation protocol used from hESC to IM. (**f**) RT–PCR at day 6 showing the expression of markers of IM (*PAX2, LHX1, OSR1*) in the presence or absence of 200 ng ml^{-1} FGF9 from day 2–6. (**g**) Quantification of the percentage of cells positive for PAX2 protein at day 6 in the presence or absence of 200 ng ml^{-1} FGF9 from day 2–6. Both differentiation protocols using BMP4/activin A (B/A) and CHIR99021 (CHIR) exceeded 80% induction efficiency. Error bars are s.d. ($n = 5$ fields in total from 3 experiments). (**h**) The presence and co-expression of PAX2 (red) and LHX1 (green) proteins at day 6 through primitive streak induction using either BMP4/activin A (B/A) or CHIR99021 (CHIR). Scale bars, 100 μm. (**i**) qRT–PCR showing the expression of markers of IM (*PAX2, LHX1*), PM (*TBX6*) and LPM (*FOXF1*) at day 6 across a concentration gradient of FGF9 from day 2 to 6. Error bars are s.d. ($n = 3$ experiments). (**j**) qRT–PCR showing the expression change of mesoderm markers at day 6 in the presence of FGF9 together with NOG or BMP4 from day 2 to 6. Error bars are s.d. ($n = 3$ experiments). (**k**) Immunofluorescence at day 6 showing a major IM population marked by PAX2 (red) and a non-overlapping PM marked by TBX6 (green). Scale bars, 100 μm. The source data for graphs are provided in Supplementary Table 1.

culture in either FGF2/BMP7 (ref. 19) or FGF9 (ref. 20). We therefore tested the capacity of three FGF family members, FGF2, FGF8 and FGF9, to induce IM from posterior primitive streak. hESC-induced posterior primitive streak was treated with 200 ng ml^{-1} of FGF2, 8 or 9 for 4 days before analysis using immunofluorescence and quantitative RT–PCR (qRT–PCR) (Fig. 1e). In the presence of FGF2 or FGF9, but not FGF8, *OSR1*, *PAX2* and *LHX1* were co-expressed with >80% of cells PAX2^{+}, suggesting differential IM induction (Fig. 1f–h). *PAX2* and *LHX1* induction in response to FGF2 or FGF9 was markedly inhibited by PD173074, a chemical inhibitor for FGFR1 and FGFR3 (Supplementary Fig. 2a,b). IM induction by FGF9 was dose dependent (optimal at 200 ng ml^{-1}) with suppression of the LPM markers, *FOXF1* (Fig. 1i) and *OSR1* (Supplementary Fig. 2b). Cellular co-localization of PAX2 and OSR1 proteins was observed after initial induction with either BMP4/activin A or CHIR99021 followed by FGF9, with LHX1 and PAX2 proteins co-localized in 79.5% (±4.7% s.d.; $n = 5$) of cells (Supplementary Fig. 2c,d). Hence, an FGF signal is sufficient to efficiently specify IM after posterior primitive streak. In early mesoderm development, BMP signalling is the key morphogen regulating lateral–medial patterning. Low BMP4 induces IM whereas high BMP4 induces LPM and NOG (noggin)-mediated antagonism of BMP signalling is required for PM (ref. 21). We reproduced this

patterning *in vitro* using BMP4 and NOG together with FGF9 (Fig. 1j). Here, *FOXF1* was effectively suppressed by NOG and the induction of IM markers *PAX2* and *LHX1* was sustained only in the presence of FGF9 alone or low NOG (Fig. 1j and Supplementary Fig. 3a,b). Although the PM marker *TBX6* behaved in a similar way to IM markers (Supplementary Fig. 3b), expression was low. Immunofluorescence revealed that $TBX6^+$ cells were a minor population completely exclusive of the $PAX2^+$ IM cells (Fig. 1k). The primitive streak can also differentiate into endoderm; however, immunofluorescence showed only 0.244% ($\pm$0.099% s.d.; $n = 5$) of cells were positive for the definitive endoderm marker, *SOX17*, confirming the specificity of differentiation into mesoderm.

In mammals, the IM differentiates into the kidney, gonad and the adrenal gland. The first structure to form is the nephric duct along which three paired excretory organs form (pronephros, mesonephros and metanephros in order from head to tail) from the same nephrogenic cord. Only the metanephros, representing the final permanent kidney, persists post birth. Key in the formation of the metanephros is reciprocal inductive events between key cellular components (Supplementary Fig. 4). The MM drives the outgrowth of the UB/ureteric epithelium (UE) through the production of GDNF. The UE promotes the survival of the MM through the production of FGF9 and induces nephron formation through Wnt signalling. After formation, each nephron elongates and segments to form the many functionally distinct cell types that comprise the nephron (Supplementary Fig. 4). On the basis of the evidence that retinoic acid (RA) can promote ureteric epithelium outgrowth[22], RA and BMP7 have previously been shown to induce renal lineages from mESCs (ref. 23) and FGF9 can maintain mouse nephron progenitors *in vitro*[20], we added 200 ng ml^{-1} FGF9, 50 ng ml^{-1} BMP7 and 0.1 μM RA from day 6 to day 17 after an initial induction using BMP4/activin A (Fig. 2a). RT–PCR across the entire differentiation protocol (Fig. 2b) revealed the stepwise differentiation from primitive streak (*MIXL1*, *LHX1*) to IM (*OSR1*, *PAX2*, *LHX1*) then MM (*SIX2*, *WT1*, *GDNF*, *HOXD11*). The expression of *HOXD11* indicated metanephros rather than mesonephros[24]. Importantly, the simultaneous induction of nephric duct/UE genes (*C-RET*; ref. 25 and *HOXB7*; ref. 26) was also observed (Fig. 2b). Indeed, immunofluorescence demonstrated the formation of $ECAD^+PAX2^+$ epithelial structures from day 14 (Fig. 2c). The formation of these early epithelial structures was promoted by RA in a dose-dependent manner (Supplementary Fig. 5b), also supporting an identity of UE (refs 22,27). Both this population and the surrounding mesenchyme showed evidence of proliferation *in vitro* (Supplementary Fig. 5a). As in the developing kidney, an initial mesenchymal field positive for SIX2 and WT1 surrounded the $ECAD^+$ UE structures (Fig. 2c,e) with this population peaking in prevalence at day 14 (Fig. 2d). The percentage of $WT1^+$ cells continued to increase after this time, possibly reflecting the expression of this protein in both nephron progenitors and more differentiated nephron structures (Fig. 2c). RT–PCR at day 22 revealed evidence for further differentiation based on the expression of podocyte (*SYNPO*, *NPHS1* and *WT1*), proximal tubule (*AQP1* and *SLC3A1*) and collecting duct genes (*AQP2* and *SCNNB1*; Supplementary Fig. 5c). Immunofluorescence confirmed the simultaneous presence of WT1 and SYNPO proteins, suggesting the formation of podocytes (Supplementary Fig. 5d) although early nephron markers were not evident.

These data suggest the coordinated differentiation of the multiple interacting cellular compartments required for kidney development. Although previous studies have used RA and BMP7 in induction protocols, our data would suggest that this may not be optimal for further differentiation. We base this on the transient expression of *SIX2*, presence of a dispersed mesenchyme and no evidence for mesenchymal *PAX2* expression, a feature of MM in the developing kidney. Addition of RA/FGF9 after an initial CHIR99021 induction generated strong UE at the expense of condensed $PAX2^+$ MM around UE (Fig. 3a). In contrast, prolonged differentiation in FGF9 alone (note the removal of all factors after day 12; Fig. 2f) also induced the stepwise induction of primitive streak, IM and both MM/UE but with a faster induction of kidney markers and a more prolonged expression of MM genes, such as *SIX2* (Fig. 2g–i). Another UE marker, GATA3, was co-expressed in the $PAX2^+$ UE and, more importantly, the MM seemed to condense tightly around the UE tips as is seen in the developing kidney (Fig. 2h,j,k). Critically, this protocol showed evidence for *PAX2* expression in both the mesenchyme and the UE (Fig. 2k) more indicative of nephrogenic potential. Finally, the expression of HOXD11 in both $WT1^+$ and $WT1^-$ cells demonstrates the additional presence of renal stroma (Fig. 3c), also supported by expression of FOXD1 (Fig. 3b).

During embryogenesis, IM also gives rise to gonad and adrenal cortex. The expression levels of markers for these tissues were no higher than is seen in human fetal kidney (Fig. 3b), suggesting that these alternative fates are not significantly selected. The transferability of this differentiation protocol from one hESC cell line to another was investigated using the H9 hESC cell line and human induced pluripotent stem cell line CRL2429 C11 (Supplementary Fig. 6). The initial induction of posterior primitive streak, subsequent induction of IM in response to FGF9 and onward differentiation was also observed using these cell lines.

The formation of what seemed to be all requisite cell populations for kidney development suggested the potential for these cells to signal between each other to generate a self-organizing tissue. Critically, this must include the formation of nephrons. To further assess the ability for this to occur, we initially examined the spontaneous differentiation of these pseudo-two-dimensional cultures using our CHIR99021–FGF9 induction protocol followed by withdrawal of growth factors from day 12–18 (Fig. 3d–f). By day 18, elongating $ECAD^+$ UE was surrounded by clumps of mesenchyme positive for three MM markers, WT1, SIX2 and PAX2 (Fig. 3d–f). This MM formed what seemed to be early nephrons/renal vesicles as indicated by JAG1 and CDH6 protein (Fig. 3f and Supplementary Fig. 4). We also observed the formation of lumens connecting UE and renal vesicle as occurs *in vivo* during nephron maturation (Fig. 3f, lower right).

Nephron formation progresses post-renal vesicle through a complicated process of segmentation, patterning and differentiation[2] with the expression of specific markers defining the identity and function of each nephron segment from the glomerulus through proximal tubule to distal tubule (Supplementary Fig. 4). To test for functional integration into kidney tissue, we used a previously characterized re-aggregation assay that represents a stringent assay of the renal potential of a test population[7,28,29] (Fig. 4a). In this assay, mouse embryonic kidneys were dissociated to single cells and then re-aggregated with either undifferentiated hESCs (control) or hESCs at day 12–13 of renal differentiation. After 4 days of culture as re-aggregates, these were sectioned and examined using

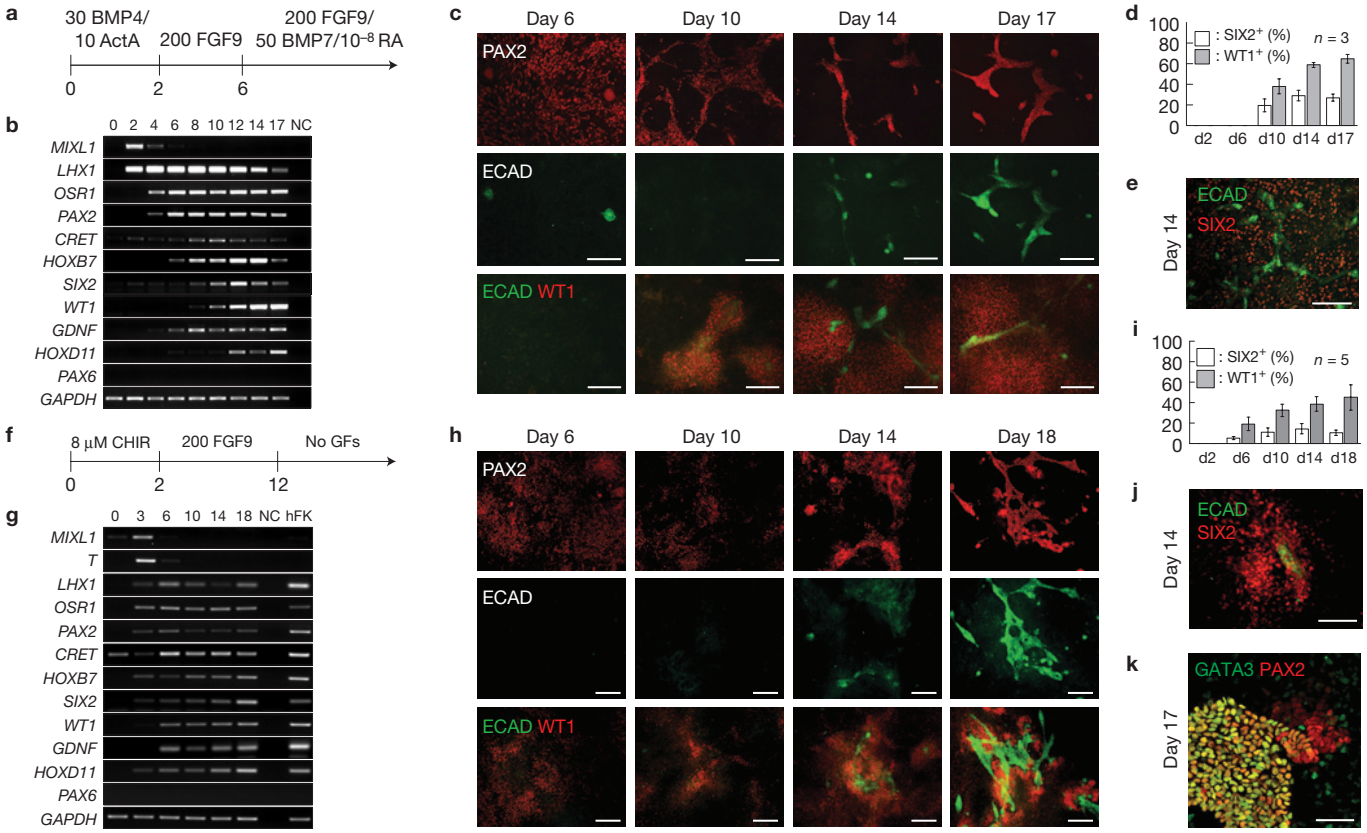

Figure 2 Stepwise temporal induction of ureteric and metanephric progenitors from hESCs *in vitro*. (**a**) Schematic representation of the initial hESC-directed differentiation protocol used to induce kidney development (BMP4/activin A–FGF9–FGF9/BMP7/RA). Numbers below the line indicate the days of differentiation. (**b**) Time-course RT–PCR from day 0 to 17 for genes representing each stage of differentiation to kidney. These include genes for primitive streak (*MIXL1, LHX1*), IM (*LHX1, PAX2, OSR1*), MM (*OSR1, SIX2, WT1, GDNF, HOXD11*) and UE (*PAX2, CRET, HOXB7*). PAX6 was included to ensure that there was no evidence for ectodermal commitment. NC, negative control with no DNA template. (**c**) Time-course immunofluorescence from day 6 to 17 showing the formation of PAX2 (red) and ECAD (green) double-positive epithelial structures (upper panels) and WT1 (red)-positive populations surrounding these epithelial structures (lower panels). Scale bars, 200 μm. (**d**) Quantification of the proportion of $WT1^+$ or $SIX2^+$ cells present within hESC cultures across the directed differentiation time course. Co-expression of these proteins marks the MM/nephron progenitor population whereas WT1 protein is also expressed in subsequently differentiating nephrons. Error bars are s.d. ($n = 3$ experiments). The source data for the graph are provided in Supplementary Table 1. (**e**) Day 14 of the differentiation revealed the presence of MM ($ECAD^-SIX2^+$) around an $ECAD^+$ UE (scale bar, 200 μm). (**f**) Schematic representation of the alternative hESC-directed differentiation protocol used to induce kidney development (CHIR99021–FGF9). Numbers below the line indicate the days of differentiation. (**g**) Time-course RT–PCR from day 0 to 18 through differentiation using CHIR99021–FGF9 representing each stage of differentiation to kidney as indicated in **b**. (**h**) Time-course immunofluorescence from day 0 to 18 through differentiation using CHIR99021–FGF9 for proteins as indicated in **c** (scale bar, 200 μm). (**i**) Quantification as described in **d** after differentiation using CHIR99021–FGF9. Error bars are s.d. ($n = 5$ fields in total from 3 experiments). (**j**) The presence of $SIX2^+$ condensed mesenchymal cells surrounding $ECAD^+$ UE structures at day 14 (scale bar, 100 μm). (**k**) Immunofluorescence microscopy at day 17 showing $PAX2^+GATA3^+$ UE at day 17 adjacent to a region of $PAX2^+GATA3^-$ MM (scale bar, 50 μm).

immunofluorescence. Cells derived from hESCs were identified using an antibody against human mitochondrial DNA (Fig. 4c arrowheads). hESC-derived cells induced using the CHIR99021–FGF9 protocol integrated into all major cellular compartments of the developing kidney, including $PAX2^+CALB^+$ UE (upper panels), $CDH6^+JAG1^+$ early nephron/renal vesicle (middle panels) and the $SIX2^+WT1^+$ nephron progenitor mesenchyme (lower panels), whereas hESC-derived cells induced using BMP4/activin A–FGF9–FGF9/BMP7/RA incorporated only into MM and UE. Such integration did not occur in re-aggregations including undifferentiated hESCs. Instead, this resulted in the complete disruption of renal development and the formation of large cysts lined with hESC-derived epithelium (Fig. 4b).

In vivo, the kidney forms in three dimensions. Isolated embryonic kidneys can grow as organoids at an air–media interface, successfully forming a branching ureteric epithelium in response to a surrounding MM and undergoing nephron formation, patterning and early segmentation. hESC differentiation was performed as monolayers, which may represent an adverse environment for self-organization and morphogenesis. To test the effect of the shape of cultures on self-organization, we lifted and replated the differentiating hESC cultures after IM commitment (day 6) at differing cell densities (Supplementary Fig. 7a) followed by continued culture as per the CHIR99021–FGF9 protocol. At day 18, cultures replated at higher density formed a uniform monolayer whereas those replated at lower density created many small, domed organoids separated across the plate. Whereas $WT1^+$ MM and $ECAD^+$ UE were present under both conditions, the smaller domed colonies formed closely packed and more advanced structures (Supplementary

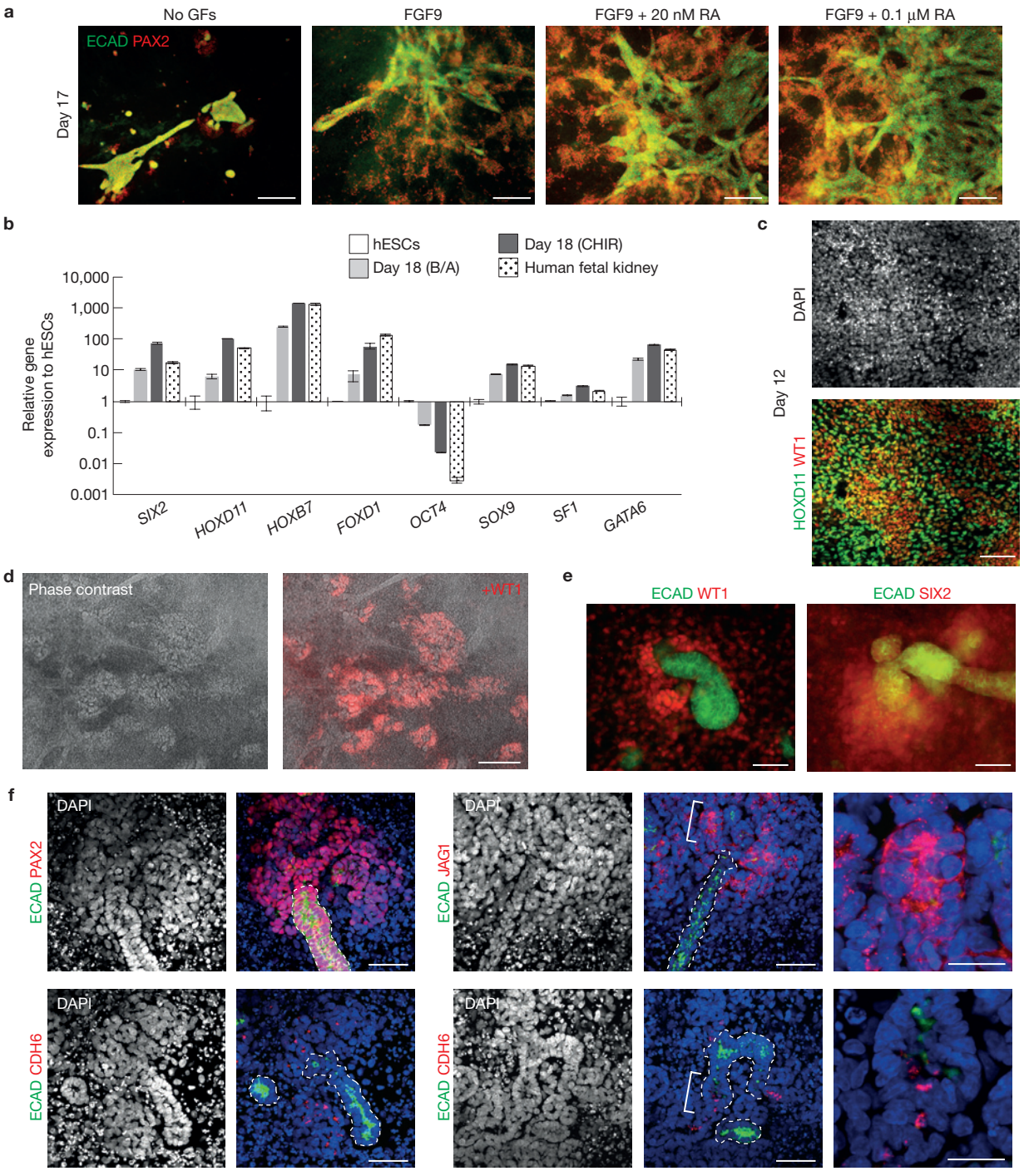

Figure 3 Assessment of renal potential and evidence for nephron induction of hESC after CHIR99021–FGF9-directed differentiation. (**a**) hESC-derived cells after day 12 of differentiation using CHIR99021–FGF9 were cultured for a further 5 days with FGF9 together with different RA concentrations or without growth factors (No GFs). Immunofluorescence for PAX2 and ECAD proteins showed that UE structures were induced in a RA dose-dependent manner (scale bar, 200 μm). (**b**) qRT–PCR for major kidney markers (*SIX2*, *HOXD11*, *HOXB7*, *FOXD1*), a pluripotent marker (*OCT4*) and gonad/adrenal cortex markers (*SOX9*, *SF1*, *GATA6*). Gene expression levels at day 18 of differentiation using either the BMP4/activin A (B/A) or CHIR99021 (CHIR) protocol were normalized to *GAPDH* and then compared with levels in undifferentiated hESCs. Human fetal kidney RNA was used as a positive control. Error bars are s.d. ($n = 3$ experiments). The source data for the graph are provided in Supplementary Table 1. (**c**) Immunofluorescence showing that at day 12 of induction, some WT1$^+$ MM cells (red) were also HOXD11$^+$ (green). HOXD11 is a specific marker of the metanephric region, including both the MM and the renal stroma (HOXD11$^+$WT1$^-$; scale bar, 200 μm). (**d**) Low-magnification view of cultures after day 18 of differentiation (CHIR99021–FGF9) using phase contrast and immunofluorescence for WT1 (red). Clusters of WT1$^+$ mesenchyme surround the UE as would be seen in an embryonic kidney (scale bar, 200 μm). (**e**) WT1$^+$ and SIX2$^+$ mesenchyme (red) tightly surrounding ECAD+ UE (green) at day 18 (scale bar, 50 μm). (**f**) Immunofluorescence confocal microscopy at day 18 showing PAX2$^+$ECAD$^+$ UE surrounded by early nephrons/renal vesicles as assessed by the presence of JAG1 and CDH6. The areas surrounded by a dashed line are PAX2$^+$GATA3$^+$ECAD$^+$ UE structures. The areas indicated by a square bracket are magnified in the next right panels (scale bar, 25 μm; magnified scale bar, 10 μm).

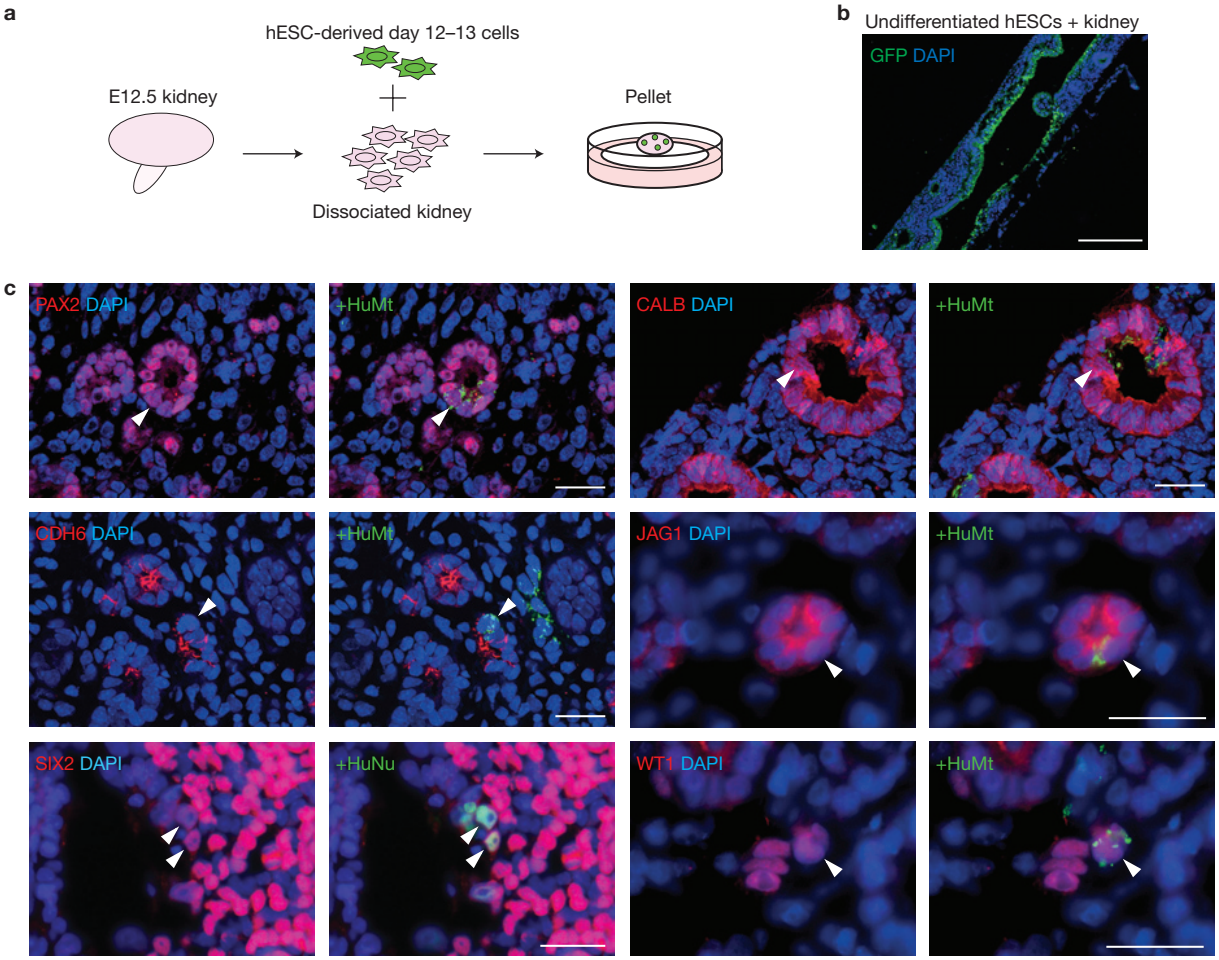

Figure 4 The integration of hESC-derived kidney progenitors into re-aggregates of mouse kidney cells. (**a**) Schematic of the re-aggregation assay of renal potential. Embryonic day 12.5–13.5 mouse kidneys were dissociated into single cells and combined with hESC-derived induced kidney cells of day 12–13, pelleted onto a filter membrane and cultured at an air–media interface for 4 days. The ratio of hESC-derived cells to mouse kidney cells was 4:96. (**b**) Re-aggregation assay using undifferentiated hESCs constitutively expressing GFP (ENVY cell line) as a negative control, showing undifferentiated hESC-derived large cyst formation (green). Scale bar, 200 μm. (**c**) Re-aggregation assay of mouse E12.5–13.5 kidney cells with hESC-derived cells after day 13 of differentiation. All integrated hESC-derived cells were detected by either human mitochondria antibody (HuMt) or a human nuclear antibody (HuNu; green). White arrowheads indicate integrated human cells into mouse renal structures. PAX2$^+$ and CALB$^+$ tubules represent UE. CDH6$^+$ and JAG1$^+$ structures represent renal vesicles. SIX2$^+$ and WT1$^+$ non-epithelial cells represent MM/nephron progenitors. All images show integration of hESC differentiated using the CHIR99021–FGF9 protocol with the exception of the integration into CALB$^+$ UE and SIX2$^+$ MM where the hESC were differentiated using the BMP4/activin A–FGF9–FGF9/BMP7/RA protocol (scale bar, 50 μm).

Fig. 7b) suggesting that the more 3D environment enhanced self-organization.

If all requisite cell populations are present for kidney morphogenesis, hESC cultures directed towards kidney differentiation should be able to form kidney organoids in the absence of any other supporting cells. To test this, hESC cultures differentiated to day 18 were enzymatically dissociated then pelleted through centrifugation before 4 days of explant culture (Fig. 5a). This represents standard culture conditions for embryonic mouse kidney explant cultures (10%FCS/DMEM without growth factors). Histological analysis of the resulting pellets revealed ECAD$^+$ tubules that exhibited either co-immunofluorescence for the UE markers PAX2 and AQP2, or the proximal tubule markers AQP1 and SLC3A1. The presence of WT1$^+$PAX2$^+$ MM surrounding the ECAD$^+$ UE was also observed, as was evidence for JAG1$^+$ECAD$^+$ renal vesicle formation (Fig. 5b hESC-derived). All of these structures were indistinguishable from the same structures formed through the dissociation and re-aggregation of normal mouse embryonic kidney (Fig. 5b, E13.5 mEK), verifying the genuine self-organization capacity of the cells present after the CHIR99021–FGF9-directed differentiation protocol. Pellets from three independent experiments were analysed with 83% revealing self-organizing structures (5/6 pellets). The same level of differentiation was not observed after BMP4/activin A–FGF9–FGF9/BMP7/RA.

The capacity of cells to 'self-organize' during both development and wound repair has long been documented[30]. During 'self-organization', distinct cell types take up specific patterns with respect to each other to create the complex structures that exist within an organ. This process is thought to involve specific cell–cell recognition and is likely to require appropriate ligand–receptor signalling and cell–matrix interactions. Recent studies in which hESCs have been induced to

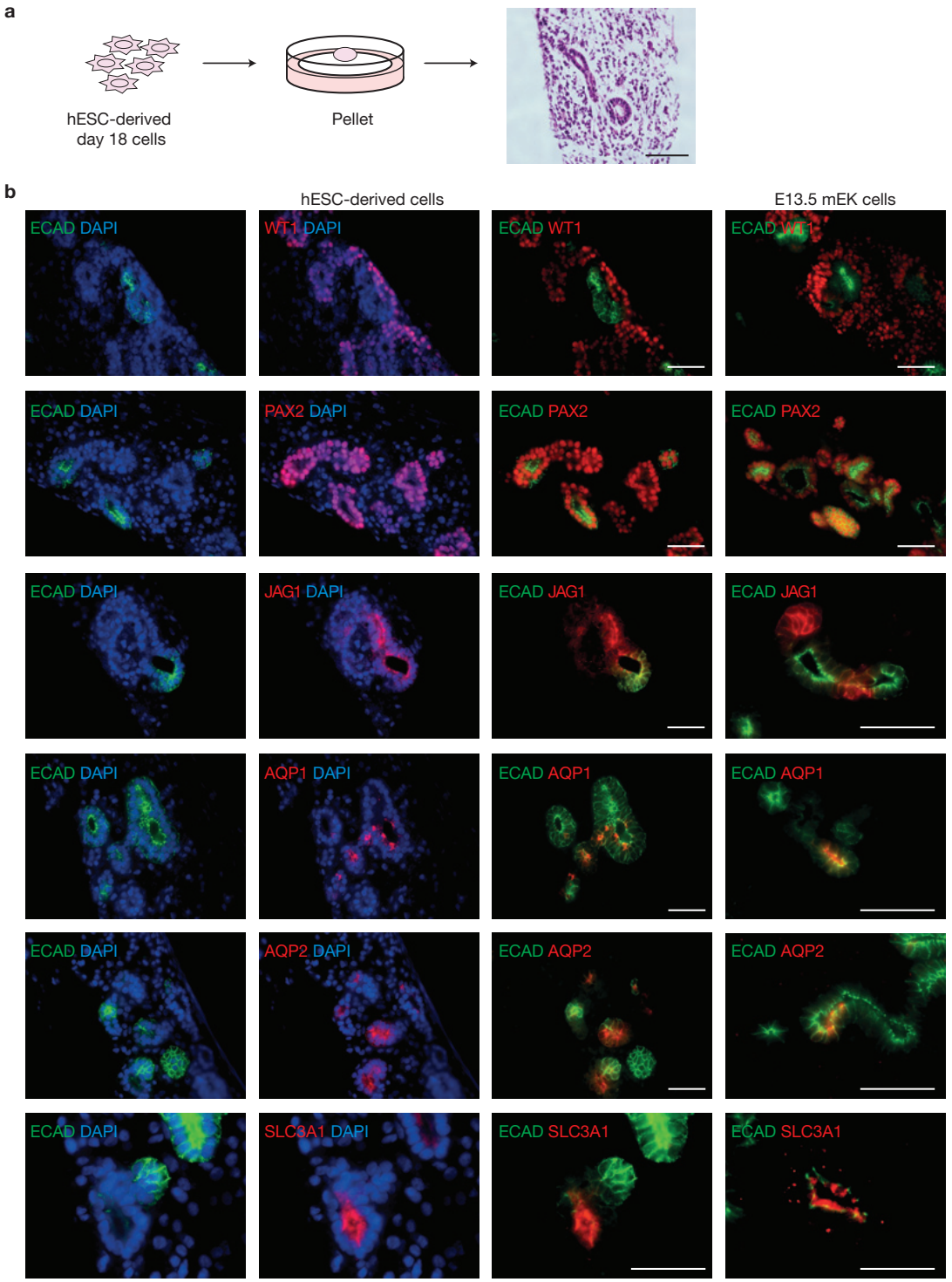

Figure 5 Evidence for self-organization after 3D culture of differentiated hESCs. (**a**) Schematic of the process used for 3D culture. hESC-derived cells after day 18 of differentiation (CHIR99021–FGF9) were collected and dissociated into single cells, pelleted and then cultured on a filter membrane at an air–media interface with 10% FCS/DMEM. After 4 days of culture, pellets were paraffin embedded and sectioned (scale bar, 200 μm). (**b**) Immunofluorescence of paraffin-embedded sections of the 3D cultured pellets showing the expression of a variety of key proteins (hESC-derived cells). ECAD (green) illustrates the presence of epithelium. $PAX2^+$ epithelium represents UE whereas $PAX2^+$ non-epithelium indicates MM and its derivatives. The co-expression of AQP2 with ECAD represents the formation of a derivative of UE, the collecting duct. WT1 staining shown here marks MM/nephron progenitors. Epithelial derivatives of MM/nephron progenitors include the renal vesicle, marked by JAG1 and proximal tubule, marked by AQP1 and SLC3A1. As a control, mouse embryonic day 13.5 kidney cells were dissociated, pelleted and then cultured in the same way as hESC-derived cells before being analysed (E13.5 mouse embryonic kidney (mEK) cells). Scale bars, 25 μm.

differentiate in culture have revealed that 3D morphogenesis of tissues as complex as optic cup, pituitary or intestine can occur through 'self-organization' of the component cells[31–33]. This implies a sophisticated capacity for a complex aggregate of cells to pattern or 'self-organize'. Several previous studies have reported the directed differentiation of hESC to IM, podocyte or proximal tubule[6,13,34,35]. None of these reported the simultaneous induction of UB- and MM-derived structures or evidence of self-organization although the growth factor regimes used were similar. Several critical differences exist in our approach. This is the first approach utilizing FGF9, which has recently been shown to be critical for MM survival. Loss of FGF9 and FGF20 results in renal agenesis and a lack of FGF9 renders the MM unable to support continued development[20]. We regard this as a critical and defining component of our protocol. Second, a stringent requirement for co-expression of combinations of genes/proteins to identify an end point, particularly at the stage of IM, has allowed us to more definitively evaluate success. In addition, we have not sorted subpopulations for subsequent differentiation, thereby allowing the influence of surrounding non-target cell types to influence the cultures as a whole. Given the described role of PM and tailbud signalling at various stages of kidney development[36,37], this may have promoted the coordinated differentiation of all communicating cell types required for formation of the kidney.

The described hESC differentiation process generates reciprocally inducing kidney progenitor populations able to self-organize to form early nephrons. This represents a significant advancement towards the generation of renal tissue from pluripotent cell sources. However, normal kidney development involves a careful balance between the self-renewal of nephron progenitors versus their differentiation into nephrons. The differentiated hESC cultures described here showed the formation of many renal vesicles but the significant loss of nephron progenitors with time, evoking the phenotype of premature progenitor differentiation seen in Six2 mutant mice[3]. This is a key challenge and suggests scope for improvement in the differentiation protocol, potentially requiring alterations to growth factors, extracellular matrix and/or oxygen tension[20,38,39] to more fully reproduce those of the embryonic kidney. A staged shift to organoid culture in bioreactors may also facilitate a more 3D environment.

In summary, here we report the successful differentiation of pluripotent cells to a self-organizing kidney. The coordinated induction of cells from the various key cellular populations involved in kidney development again demonstrates the requirement for interacting niches for the creation of complex morphogenetic structures. The capacity for such populations to undergo self-organization *in vitro* bodes well for the future of tissue/organ bioengineering. The fact that we can form organoids from differentiated hESC cultures alone opens the possibility of generating tissue-based nephrotoxicity screens, *in vitro* disease models or developing transplantable organoids to supplement renal function. It also suggests the feasibility of generating specific mature renal cell types for later purification. □

METHODS

Methods and any associated references are available in the online version of the paper.

Note: Supplementary Information is available in the online version of the paper

ACKNOWLEDGEMENTS

We are grateful to E. Wolvetang for providing an iPSC line and D. Titmarsh, A. Hidalgo-Gonzalez and J. Cooper-White for supportive comments. This work was supported by the Queensland State Government through a National/International Research Alliance Project, the Australian Research Council as part of the Stem Cells Australia Strategic Research Initiative (SRI110001002) and the National Health and Medical Research Council of Australia (APP1041277). M.H.L. is a Senior Principal Research Fellow of the NHMRC.

AUTHOR CONTRIBUTIONS

M.T. and M.H.L. conceived and planned the project and wrote the manuscript. M.B. and P.X.E. provided technical assistance with hESC culture, histology, microscopy and differentiation protocols. E.G.S. and A.G.E. provided targeted hESC lines and advised on design and execution. J.M.V. provided technical advice, support and analysis for *ex vivo* recombination assays.

COMPETING FINANCIAL INTERESTS

M.H.L. consults for Organovo Inc.

Published online at www.nature.com/doifinder/10.1038/ncb2894
Reprints and permissions information is available online at www.nature.com/reprints

1. Little, M. H. & McMahon, A. P. Mammalian kidney development: principles, progress, and projections. *Cold Spring Harb. Perspect. Biol.* **4** (5) (2012).
2. Tam, P. P. & Loebel, D. A. Gene function in mouse embryogenesis: get set for gastrulation. *Nat. Rev. Genet.* **8,** 368–381 (2007).
3. Kobayashi, A. *et al.* Six2 defines and regulates a multipotent self-renewing nephron progenitor population throughout mammalian kidney development. *Cell Stem Cell* **3,** 169–181 (2008).
4. Rumballe, B. A. *et al.* Nephron formation adopts a novel spatial topology at cessation of nephrogenesis. *Dev. Biol.* **360,** 110–122 (2011).
5. Lusis, M., Li, J., Ineson, J. & Little, M. H. Isolation of clonogenic, long-term self-renewing renal stem cells. *Stem Cell Res.* **5,** 23–39 (2010).
6. Takasato, M., Maier, B. & Little, M. H. Recreating kidney progenitors from pluripotent cells. *Pediatr. Nephrol.* http://dx.doi.org/10.1007/s00467-013-2592-7 (2013).
7. Gadue, P., Huber, T. L., Paddison, P. J. & Keller, G. M. Wnt and TGF-beta signaling are required for the induction of an *in vitro* model of primitive streak formation using embryonic stem cells. *Proc. Natl Acad. Sci. USA* **103,** 16806–16811 (2006).
8. Soares, M. L. *et al.* Functional studies of signaling pathways in peri-implantation development of the mouse embryo by RNAi. *BMC Dev. Biol.* **5,** 28 (2005).
9. Lu, C. C. & Robertson, E. J. Multiple roles for Nodal in the epiblast of the mouse embryo in the establishment of anterior–posterior patterning. *Dev. Biol.* **273,** 149–159 (2004).
10. Sumi, T., Tsuneyoshi, N., Nakatsuji, N. & Suemori, H. Defining early lineage specification of human embryonic stem cells by the orchestrated balance of canonical Wnt/beta-catenin, Activin/Nodal and BMP signaling. *Development* **135,** 2969–2979 (2008).
11. Davis, R. P. *et al.* Targeting a GFP reporter gene to the MIXL1 locus of human embryonic stem cells identifies human primitive streak-like cells and enables isolation of primitive hematopoietic precursors. *Blood* **111,** 1876–1884 (2008).
12. Ng, E. S., Davis, R., Stanley, E. G. & Elefanty, A. G. A protocol describing the use of a recombinant protein-based, animal product-free medium (APEL) for human embryonic stem cell differentiation as spin embryoid bodies. *Nat. Protoc.* **3,** 768–776 (2008).
13. Mae, S. *et al.* Monitoring and robust induction of nephrogenic intermediate mesoderm from human pluripotent stem cells. *Nat. Commun.* **4,** 1367 (2013).
14. James, R. G. *et al.* Odd-skipped related 1 is required for development of the metanephric kidney and regulates formation and differentiation of kidney precursor cells. *Development* **133,** 2995–3004 (2006).
15. Tsang, T. E. *et al.* Lim1 activity is required for intermediate mesoderm differentiation in the mouse embryo. *Dev. Biol.* **223,** 77–90 (2000).
16. Torres, M., Gómez-Pardo, E., Dressler, G. R. & Gruss, P. Pax-2 controls multiple steps of urogenital development. *Development* **121,** 4057–4065 (1995).
17. Crossley, P. H. & Martin, G. R. The mouse Fgf8 gene encodes a family of polypeptides and is expressed in regions that direct outgrowth and patterning in the developing embryo. *Development* **121,** 439–451 (1995).
18. Colvin, J. S. *et al.* Genomic organization and embryonic expression of the mouse fibroblast growth factor 9 gene. *Dev. Dynam.* **216,** 72–88 (1999).
19. Dudley, A. T., Godin, R. E. & Robertson, E. J. Interaction between FGF and BMP signaling pathways regulates development of metanephric mesenchyme. *Genes Dev.* **13,** 1601–1613 (1999).
20. Barak, H. *et al.* FGF9 and FGF20 maintain the stemness of nephron progenitors in mice and man. *Dev. Cell* **22,** 1191–1207 (2012).
21. James, R. G. & Schultheiss, T. M. Bmp signaling promotes intermediate mesoderm gene expression in a dose-dependent, cell-autonomous and translation-dependent manner. *Dev. Biol.* **288,** 113–125 (2005).
22. Rosselot, C. *et al.* Non-cell-autonomous retinoid signaling is crucial for renal development. *Development* **137,** 283–292 (2010).

23. Kim, D. & Dressler, G. R. Nephrogenic factors promote differentiation of mouse embryonic stem cells into renal epithelia. *J Am. Soc. Nephrol.* **16,** 3527–3534 (2005).
24. Mugford, J. W. *et al*. Hoxd11 specifies a program of metanephric kidney development within the intermediate mesoderm of the mouse embryo. *Dev. Biol.* **319,** 396–405 (2008).
25. Pachnis, V., Mankoo, B. & Costantini, F. Expression of the c-ret proto-oncogene during mouse embryogenesis. *Development* **119,** 1005–1017 (1993).
26. Srinivas, S. *et al*. Expression of green fluorescent protein in the ureteric bud of transgenic mice: a new tool for the analysis of ureteric bud morphogenesis. *Dev. Genet.* **24,** 241–251 (1999).
27. Mendelsohn, C. *et al*. Stromal cells mediate retinoid-dependent functions essential for renal development. *Development* **126,** 1139–1148 (1999).
28. Davies, J. A. *et al*. Dissociation of embryonic kidney followed by re-aggregation as a method for chimeric analysis. *Methods Mol. Biol.* **886,** 135–146 (2012).
29. Hendry, C. E. & Vanslambrouck, J. M. *et al*. Direct transcriptional reprogramming of adult cells to embryonic nephron progenitors. *J. Am. Soc. Nephrol.* **24,** 1424–1434 (2013).
30. Trinkaus, J. P. & Groves, P. W. Differentiation in culture of mixed aggregates of dissociated tissue cells. *Proc. Natl Acad. Sci. USA* **41,** 787–795 (1955).
31. Suga, H. *et al*. Self-formation of functional adenohypophysis in three-dimensional culture. *Nature* **480,** 57–62 (2011).
32. Eiraku, M. *et al*. Self-organizing optic-cup morphogenesis in three-dimensional culture. *Nature* **472,** 51–56 (2011).
33. Spence, J. R. *et al*. Directed differentiation of human pluripotent stem cells into intestinal tissue *in vitro*. *Nature* **470,** 105–108 (2011).
34. Narayanan, K. *et al*. Human embryonic stem cells differentiate into functional renal proximal tubular-like cells. *Kidney Int.* **83,** 593–603 (2013).
35. Song, B. *et al*. The directed differentiation of human iPS cells into kidney podocytes. *PLoS ONE* **7,** e46453 (2012).
36. Brenner-Anantharam, A. *et al*. Tailbud-derived mesenchyme promotes urinary tract segmentation via BMP4 signaling. *Development* **134,** 1967–1975 (2007).
37. Guillaume, R., Bressan, M. & Herzlinger, D. Paraxial mesoderm contributes stromal cells to the developing kidney. *Dev. Biol.* **329,** 169–175 (2009).
38. Uchiyama, Y. *et al*. Kif26b, a kinesin family gene, regulates adhesion of the embryonic kidney mesenchyme. *Proc. Natl Acad. Sci. USA* **107,** 9240–9245 (2010).
39. Linton, J. M., Martin, G. R. & Reichardt, L. F. The ECM protein nephronectin promotes kidney development via integrin alpha8beta1-mediated stimulation of Gdnf expression. *Development* **134,** 2501–2509 (2007).

METHODS

hESC culture and differentiation. HES3 (*MIXL1*$^{GFP/wt}$) cells were routinely cultured on irradiated mouse embryonic fibroblast feeder cells in F12/DMEM (Life Technologies) supplemented with 20% KnockOut serum replacement (Life Technologies), 100 μM MEM NEAA (Life Technologies), 110 μM 2-mercaptoethanol (Life Technologies), 1× penicillin/streptomycin (Life Technologies), 1× Glutamax (Life Technologies) and 10 ng ml^{-1} bFGF (R&D systems). The day before starting differentiation, cells were plated at 12,000–15,000 cells cm^{-2} on a Matrigel-coated 96-well plate. After overnight culture, cells were exposed to 30 ng ml^{-1} BMP4 (R&D Systems) and 10 ng ml^{-1} activin A (R&D Systems) or 8 μM CHIR99021 in a previously established serum-free media APEL for 2–3 days, then 200 ng ml^{-1} FGF9 and 1 μg ml^{-1} heparin in APEL media for 4 days to induce IM cells. Subsequently cells were exposed to 200 ng ml^{-1} FGF9, 50 ng ml^{-1} BMP7, 0.1 μM RA and 1 μg ml^{-1} heparin for 4–11 days in case of BMP4/activin A induction. In case of CHIR99021 induction, cells were exposed to 200 ng ml^{-1} FGF9 and 1 μg ml^{-1} heparin for 6 days then cultured in APEL basal media for another 6 days. Media were changed every 2 days.

Fluorescence-activated cell sorting. Cell suspension was prepared from undifferentiated or differentiated hESCs. hESCs were collected with TripLE Select (Life Technologies) at 37 °C for 5 min and dissociated using fine-tipped pipettes. After the cells had been filtered through a 40 μm nylon mesh, they were resuspended in PBS containing 0.5% FCS and 1 mM EDTA at a final density of 2×10^6 cells ml^{-1}. Propidium iodide (Sigma) was added at a final concentration of 50 mg ml^{-1} to label the dead cells. FACS analyses were done with the FACS Aria (Becton Dickinson). Dead cells were excluded from the plots on the basis of propidium iodide staining. All FACS analyses were successfully repeated more than three times and representative results are shown.

Immunocytochemistry. Cells were fixed with 4% paraformaldehyde in PBS for 10 min at 4 °C followed by a wash with PBS. Then cells were blocked with 1% BSA, 0.2% milk, 0.3% Triton X/PBS for 1 h at room temperature and incubated with primary antibodies overnight at 4 °C. Secondary antibodies were incubated for 1 h at room temperature. The following antibodies and dilutions were used: rabbit anti-PAX2 (1:200, #71-6,000, Zymed Laboratories), goat anti-OSR1 (1:75, #sc-67723, Santa Cruz Biotechnology), goat anti-LHX1 (1:75, #sc-19341, Santa Cruz Biotechnology), mouse anti-TBX6 (1:200, AF4744, R&D Systems), goat anti-SOX17 (1:200, #AF1924, R&D Systems), rabbit anti-SIX2 (1:200, #11562-1-AP, Proteintech), mouse anti-ECAD (1:200, #610181, BD Biosciences), rabbit anti-WT1 (1:100, #sc-192, Santa Cruz Biotechnology), mouse anti-HOXD11 (1:200, #SAB1403944, Sigma-Aldrich), goat anti-GATA3 (1:200, AF2605, R&D Systems), rabbit anti-JAG1 (1:200, #ab7771, Abcam), rabbit anti-CDH6 (1:100, #HPA007047, Sigma Aldrich) and goat anti-SYNPO (1:200, #sc-21537, Santa Cruz Biotechnology). Secondary antibodies were: Alexa-488-conjugated goat anti-rabbit, Alexa-594-conjugated donkey anti-rabbit, Alexa-488-conjugated donkey anti-goat and Alexa-594-conjugated goat anti-mouse (1:250, Life Technologies). Images were taken using a Nikon Ti-U microscope or a Zeiss LSM 510 Meta ultraviolet confocal microscope. All immunofluorescence analyses were successfully repeated more than three times and representative images are shown.

Immunofluorescence. Pellets were fixed with 4% PFA for 10 min at 4 °C, embedded in paraffin and sectioned with 7 μm thickness. Sections were blocked with sheep serum for 1 h at room temperature, and then antigen retrieval was performed using Antigen Unmasking Solution (Vector Labs). Primary antibodies were incubated overnight at 4 °C and secondary antibodies were incubated for 1 h at room temperature. The following antibodies and dilutions were used: rabbit anti-CALB1 (1:200, #C2724, Sigma-Aldrich), rabbit anti-AQP1 (1:200, sc-20810, Santa Cruz Biotechnology), rabbit anti-AQP2 (1:200, AB3274, Millipore), rabbit anti-SLC3A1 (1:100, 16343-1-AP, Proteintech) and rabbit anti-human specific mitochondria (HuMt; 1:800, #ab92824, Abcam). Frozen sections embedded in OCT compound (Sakura) were used for staining with anti-human specific nuclei (HuNu; 1:800, #MAB1281, Merck). Images were taken using an Olympus BX-51 microscope or a Zeiss LSM 510 Meta ultraviolet confocal microscope. All immunofluorescence analyses were successfully repeated more than three times and representative images are shown.

Gene expression analysis. Total RNA was extracted from cells using RNeasy micro kit (QIAGEN) and cDNA was synthesized from >100 ng RNA using Super Script III reverse transcriptase (Life Technologies). qRT–PCR analyses were performed with Syber Green (Applied Biosystems) by an ABI PRISM 7500 real-time PCR machine. All absolute data were first normalized to GAPDH and then normalized to control samples (δ–δ-Ct method). Conventional RT–PCR analyses were performed using OneTaq DNA polymerase (NEB) as per the manufacturer's instruction. All RT–PCR analyses were successfully repeated more than three times and representative images are shown. The sequences of primers used for RT–PCR and qRT–PCR are as listed in Supplementary Table 2.

Quantification of proportion of induced cells. To quantify the proportion of differentiated cells positive for PAX2$^+$, LHX1$^+$, SOX17$^+$, SIX2$^+$ or WT1$^+$, cells were immunofluorescently stained with each antibody together with the nuclear stain DAPI. The ratio of differentiated cells to total cells was manually counted using ImageJ in 1 or 2 representative fields per experiment (total 3–5 representative fields from thee independent experiments, 1–1.5 × 10^3 cells in total), using an Olympus BX-51 microscope, ×10 objective.

3D cultures. hESC-derived induced kidney cells were collected and dissociated into single cells using TripLE select (Life Technologies) at day 12–13 of the differentiation. Cells (10×10^5) were spun down at ×400*g* for 2 min to form a pellet and then placed onto a filter membrane with 0.4 μm pores of 13 mm diameter (#7060-1304 Whatman) with a collagen IV (Becton Dickinson) coat at 10 μg cm^{-2}. The filter was floated on the culture media of 10% FCS/DMEM for 4 days.

Re-aggregation assay. The re-aggregation assay was performed as previously described[5,29]. Briefly, a filter membrane was coated with collagen IV (Becton Dickinson) at 10 μg cm^{-2}. For preparing the embryonic kidney cells to be recombined, embryonic kidneys from 12.5–13.5-dpc (days post coitum) mice were digested with Accutase (Life Technologies) at 37 °C for 10 min and dissociated by manually pipetting. After the cells had been filtered through a 100 μm nylon mesh, 4–10 × 10^5 of embryonic kidney cells were recombined with 4% of hESC-derived cells and then centrifuged at ×400*g* for 2 min to form a pellet. The pellet was placed on a filter membrane prepared as above and cultured for 4 days with 10% FCS/DMEM culture media.

DOI: 10.1038/ncb2894

nature cell biology

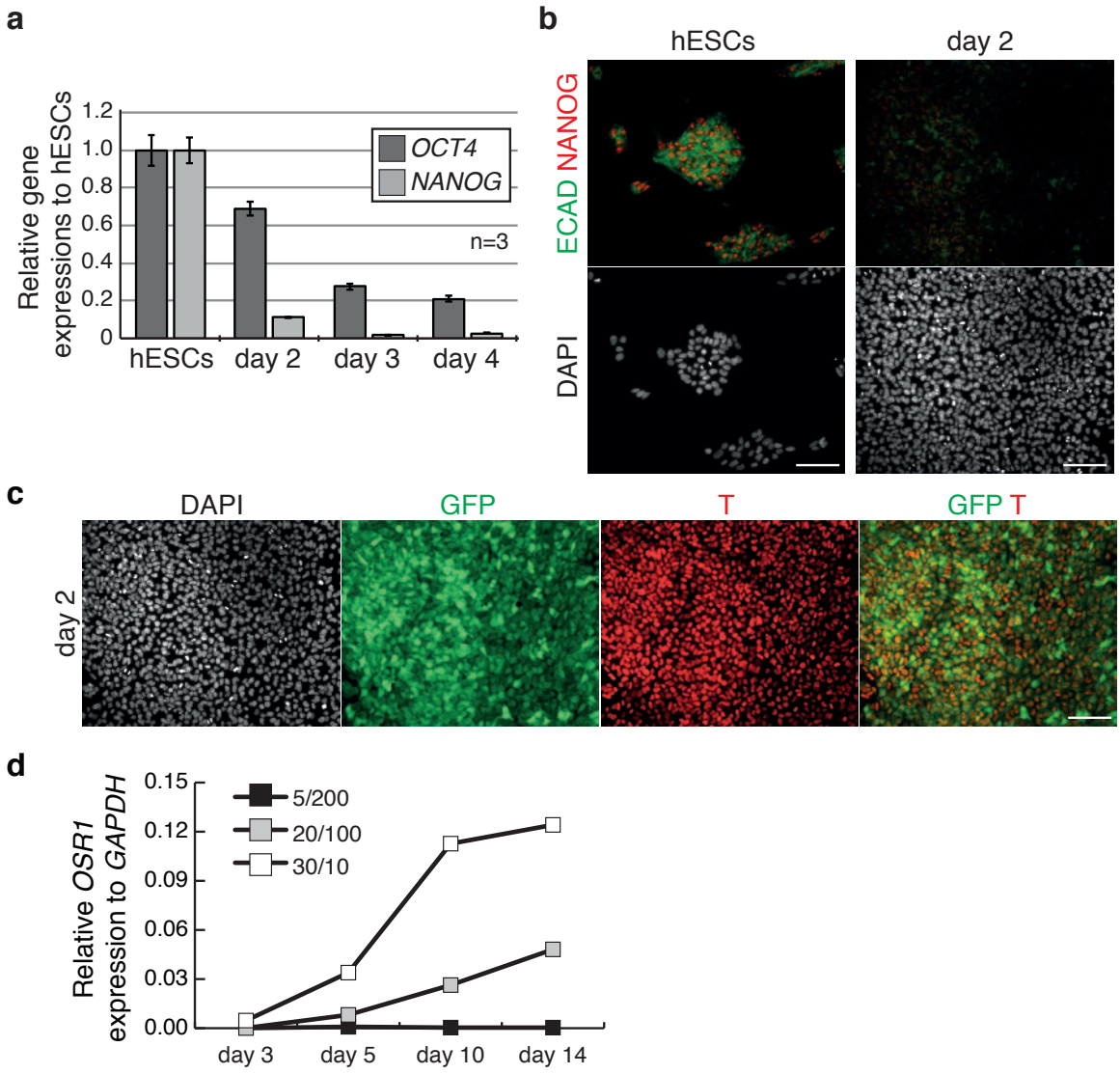

Supplementary Figure 1 Posterior primitive streak induction. **a,** Time course quantitative RT-PCR for pluripotent markers, *OCT4* and *NANOG* after induction with BMP4/ActivinA (30/10 ng/ml), showing a reduction in pluripotent gene expression with time. Error bars are s.d. (n=3 experiments). The source data for the graph are provided in Supplementary Table 1. **b,** IF for markers of ES cells, NANOG and ECAD, before (hESCs) and after (day 2) primitive streak induction using CHIR99021. (scale = 100㎜) **c,** IF for markers of posterior primitive streak, T and MIXL1 (GFP), after the primitive streak induction (day 2) using CHIR99021. MIXL1 was detected as GFP expression driven by the MIXL1 endogenous promoter. (scale = 100㎜) **d,** Levels of spontaneous *OSR1* expression induced across time after culture if 3 different ratios of BMP4 and Activin A (ng/mL). hESCs were formed embryoid bodies with 3 different ratios of BMP4 and Activin A for 3 days then spontaneously differentiated under no growth factor condition until day 14. This demonstrates improved *OSR1* expression in cells induced with high BMP4 and low Activin A (30/10). *OSR1* marks IM and LPM.

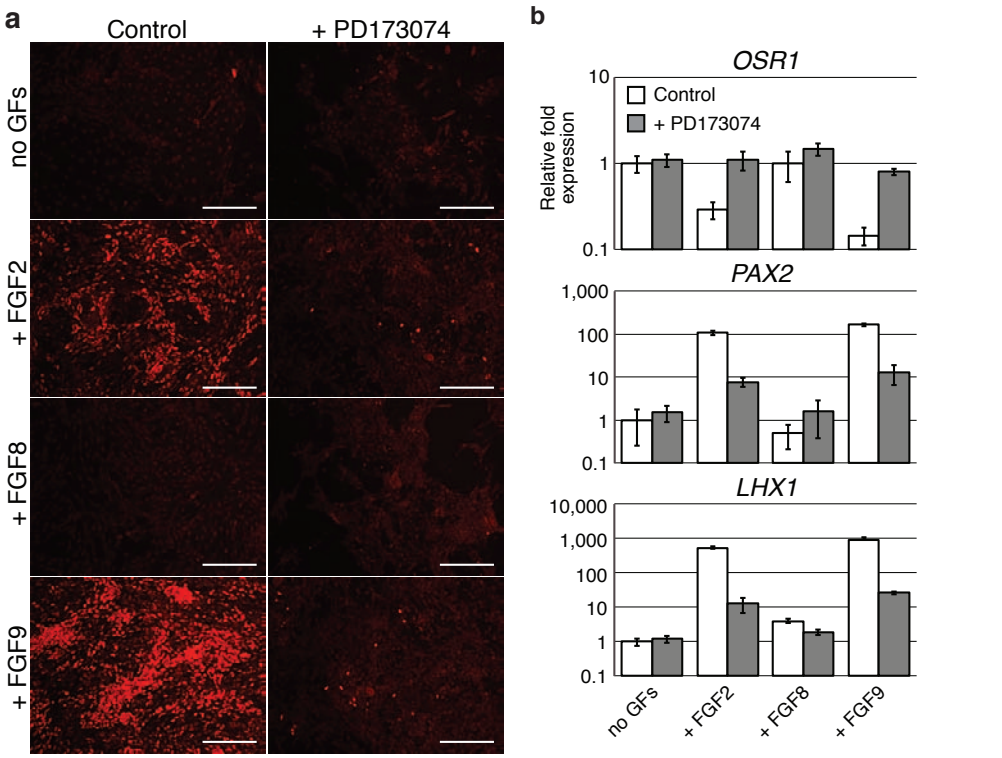

d

	%PAX2$^-$	%PAX2$^+$	
total	13.6 ± 5.5	86.4 ± 5.5	
%LHX1$^-$	13.3 ± 5.2	6.8 ± 2.9	
%LHX1$^+$	0.4 ± 0.5	79.5 ± 4.7	(n=5)

Supplementary Figure 2 Influence of FGF signaling on induction of IM proteins. **a,** IF for PAX2 protein on hESC cultures at day 6 treated with BMP4/Activin A to day 2 and FGF2 (200ng/ml), FGF8 (200ng/ml), FGF9 (200ng/ml) or no growth factors (no GFs) from day 2 to 6 in the presence or absence of the FGF signaling inhibitor, PD173074. (scale = 200㎜) **b,** Quantitative RT-PCR to examine the relative expression level of *PAX2, LHX1* and *OSR1* at day 6 of the same protocol as IF (a). Shaded bars show the effect of addition of the FGF inhibitor, PD173074. Error bars are s.d. (n=3 experiments). The source data for graphs are provided in Supplementary Table 1. **c,** IF for the IM marker PAX2 and the marker of both LPM and IM, OSR1, on hESC cultures at day 6 treated with BMP4/Activin A (+FGF9 (B/A)) or 8 μM CHIR99021 (+FGF9 (CHIR)) to day 2 followed by 200 ng/mL FGF9 or no growth factors (no GFs) from day 2 to 6. Secondary antibody only control was used as a negative control (2º Ab only) (scale = 100㎜) The source data for graphs are provided in Supplementary Table 1. **d,** A table showing the percent of PAX2$^-$ and PAX2$^+$ cells in total (total) or together with LHX1$^-$ and LHX1$^+$ cells on hESC cultures at day 6 treated with 8 μM CHIR99021 to 2 days followed by 200 ng/mL FGF9 from day 2 to 6. Errors are s.d. (n=5 fields in total from 3 experiments).

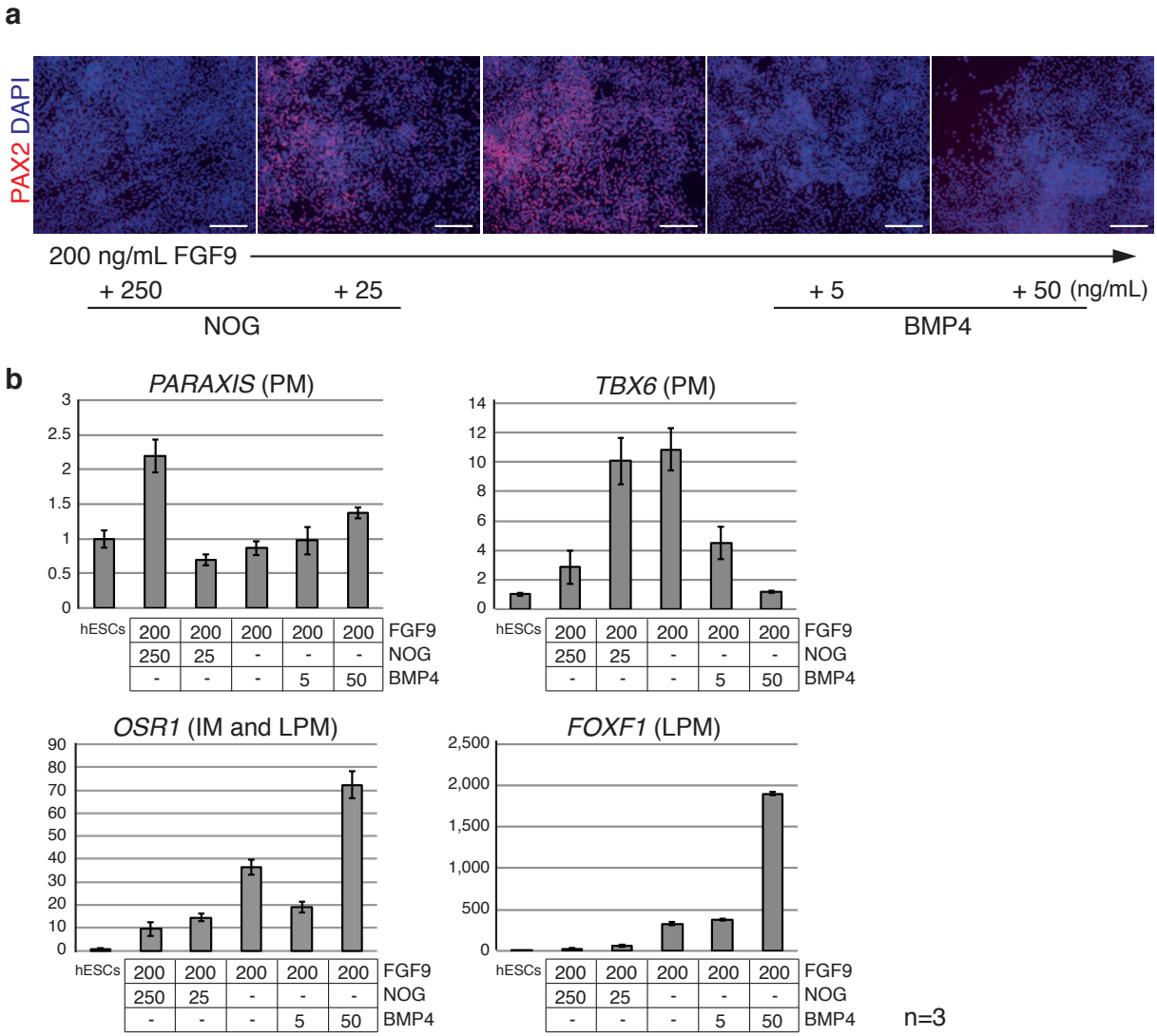

Supplementary Figure 3 The effect of BMP signaling on lateral-medial patterning of early mesoderm. **a,** IF for DAPI (blue) and PAX2 (red) at day 6 in the presence of 200ng/mL FGF9 with or without BMP4 (5 or 50ng/mL) or the BMP antagonist NOG (25 or 250ng/mL) from day 2 to day 6. (scale = 200㎛) **b,** qRT-PCR to investigate the effect of this BMP/NOG gradient on the expression of PM (*PARAXIS* and *TBX6)* and LPM (*FOXF1* and *OSR1)* markers at day 6. Error bars are s.d. (n=3 experiments). The source data for graphs are provided in Supplementary Table 1.

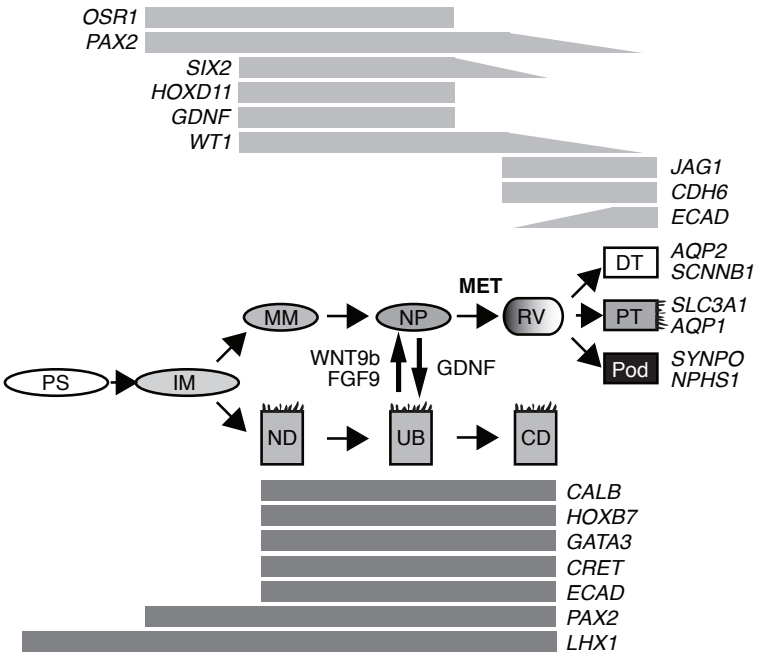

Supplementary Figure 4 Schematic illustrating the anticipated gene expression of distinct progenitor and derivative cell populations during early kidney development. PS, primitive streak; IM, intermediate mesoderm; MM, metanephric mesenchyme; NP, nephron progenitor / nephrogenic mesenchyme; RV, renal vesicle; DT, distal convoluted tubule; PT, proximal convoluted tubule; Pod, podocyte; ND, nephric duct; UB, ureteric bud / ureteric epithelium; CD, collecting duct; MET, mesenchymal to epithelial transition. All genes are indicated in italics. Shaded boxes indicate the timing and duration of expression for adjacent labeled genes. Specific genes marking DT, PT and Pod are indicated next to each cell type. The reciprocal induction of differentiation known to occur between the UB and NP is supported by the expression of *FGF9* (nephrogenic mesenchyme survival) and *Wnt9b* (MET) and from the UB and *GDNF* (ureteric branching) by the NP.

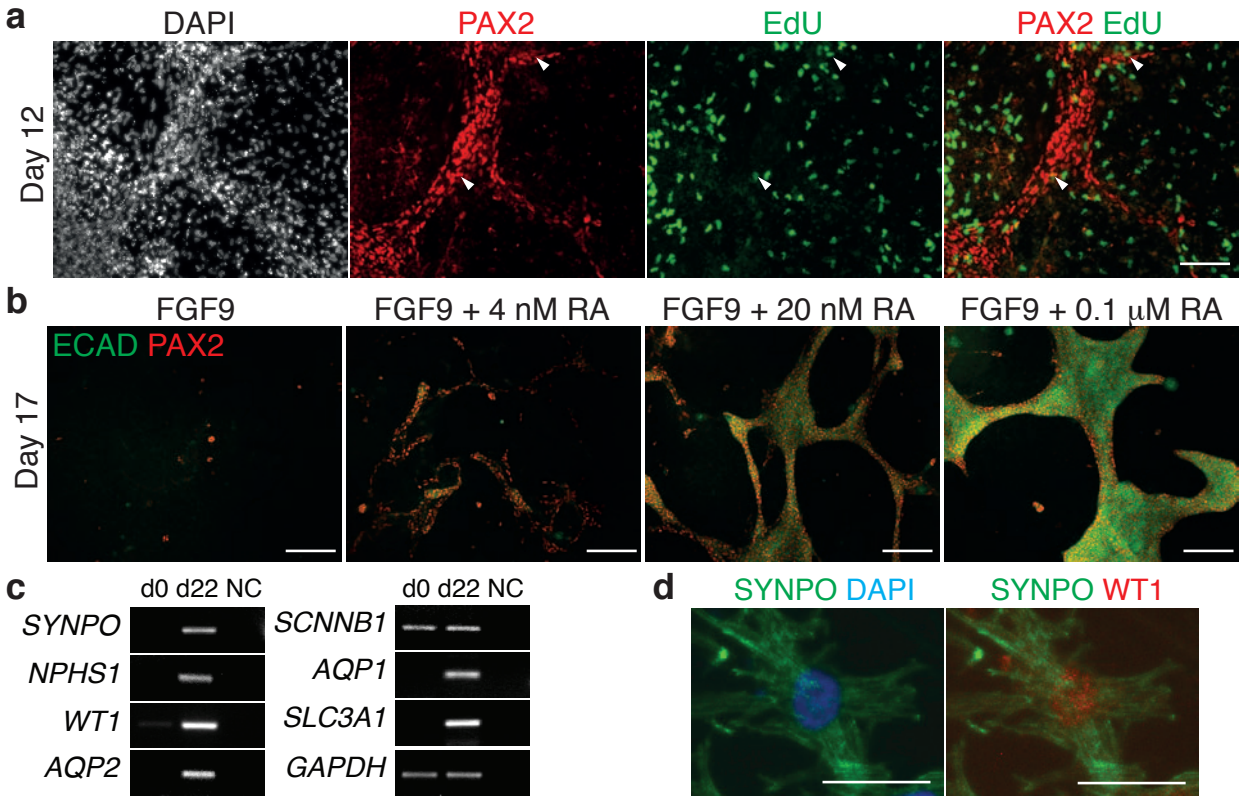

Supplementary Figure 5 The positive effect of RA on ureteric epithelium formation. **a,** EdU incorporation assay at day 12 of differentiation. 30 min exposure by EdU revealed that not only PAX2$^+$ pre-epithelium structures but also PAX2 negative cells are proliferating. White arrowheads indicate EdU incorporation in PAX2$^+$ cell. (scale = 100㎜) **b,** IM cells at day 6 after primitive streak induction using BMP4/Activin A were cultured for 11 days with FGF9 together with different RA concentrations. IF for UE markers, PAX2$^+$ECAD$^+$, showed UE structures were induced in a RA dose-dependent manner. (scale = 200㎜) **c,** RT-PCR at day 22 of differentiation using BMP4:Activin A/FGF9/FGF9:BMP7:RA protocol revealed the expression of genes indicative of differentiation into mature renal cell types, including *SYNPO, NPHS1* and *WT1* for podocyte; *AQP2* and *SCNNB1* for distal tubule or collecting duct and *AQP1* and *SLC3A1* for proximal tubule. NC, negative control with no DNA template. **g,** IF of day 22 differentiation using BMP4/Activin A showing co-expression of two key podocyte markers; the slit-diaphragm protein SYNPO (green) and nuclear WT1 (red). Nuclei are also stained with DAPI (blue). (scale = 50㎜) The source data for graphs are provided in Supplementary Table 1.

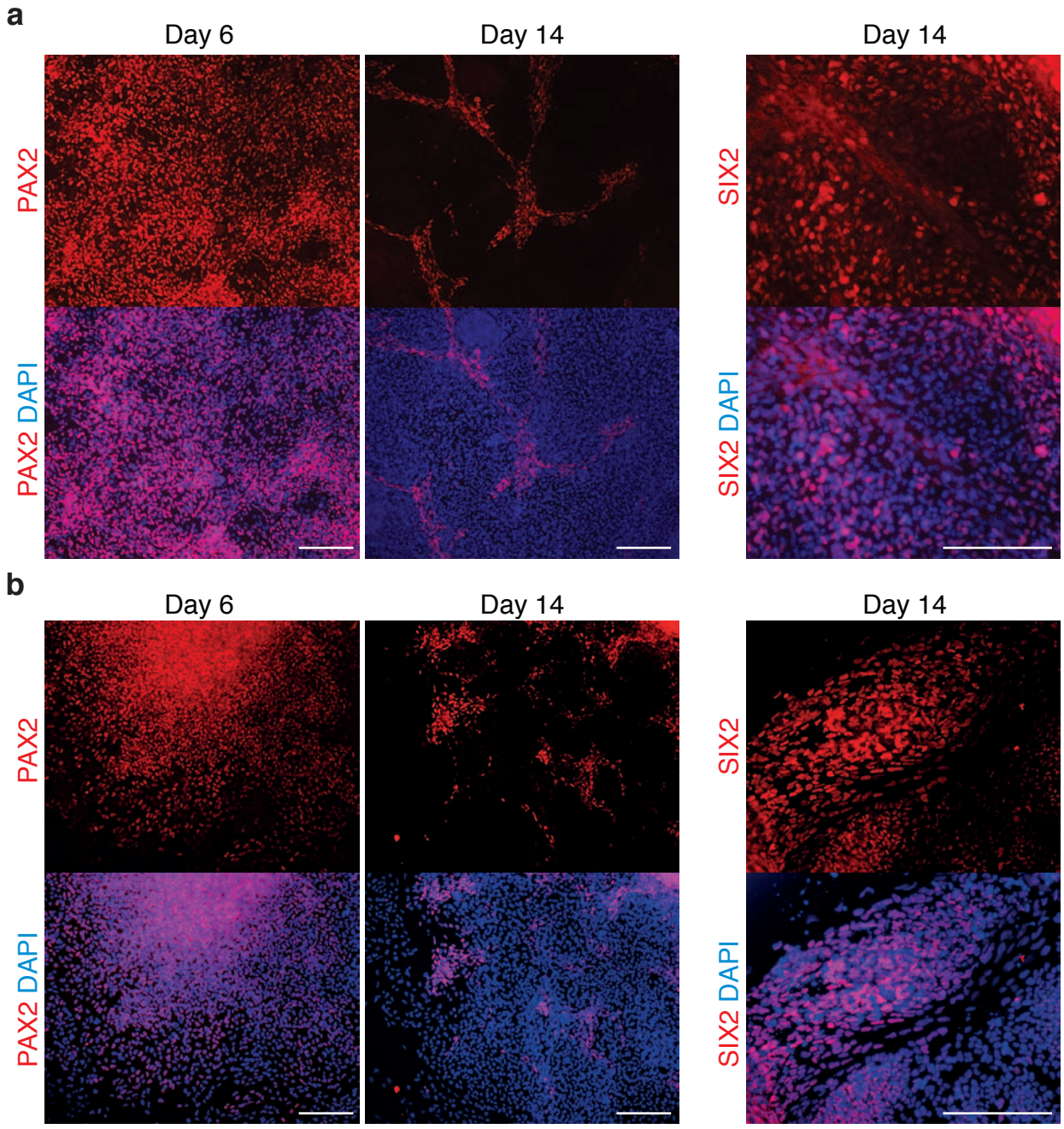

Supplementary Figure 6 Differentiation of H9 hES cell line and iPS cell line towards renal lineages. **a, b,** Immunofluorescence for DAPI (blue), PAX2 (red) or SIX2 (red) at Day 6 and Day 14 of differentiation on H9 hESC (a) and CRL2429 C11 iPS cells (b). (scale = 200mm).

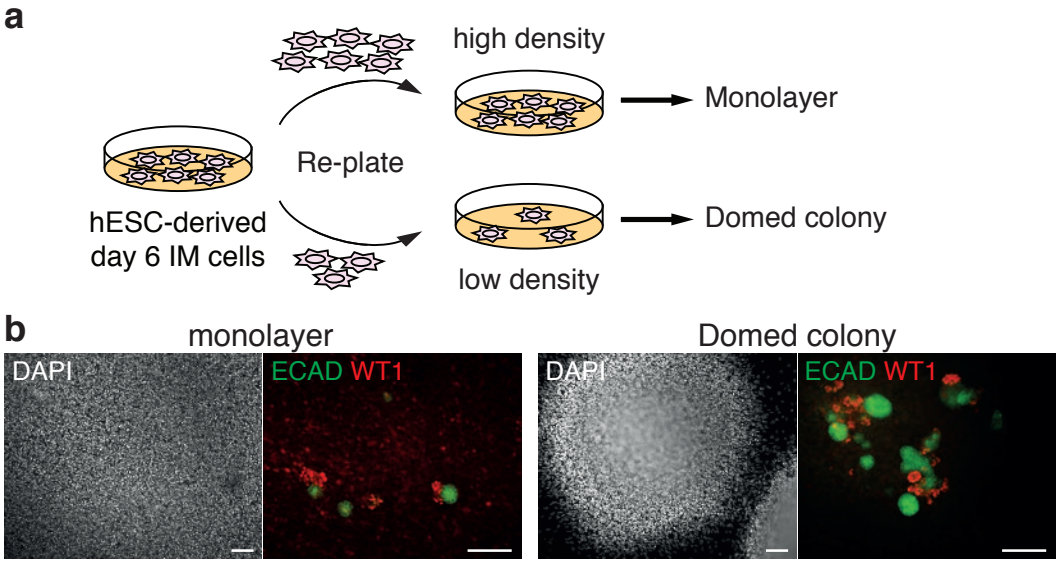

Supplementary Figure 7 The effect of 3D culture environment on self-organisation events. **a,** Schematic of the replating assay. IM cells at day 6 were harvested and re-plated at high density or low density. Then cells were cultured for 12 days (6 days with 200 ng/mL FGF9 then another 6 days without growth factors). Cells plated at high density formed a uniform layer of cells while those plated at low density formed domed colonies. **b,** Induced IM cells at day 6 were re-plated to form monolayer or domed colonies at day 18. Cells were stained with ECAD for UE and WT1 for MM. More advanced structures are seen within domed colonies possibly due to the proximity of reciprocally inductive cell populations. (scale = 100㎜).

Supplementary Table Legends

Supplementary Table 1 The source data for graphs.

Supplementary Table 2 Sequences of PCR primers used for both RT-CR and qRT-PCR analyses of gene expression.